Nonlinear damage rheology and wave resonance in rocks

V. Lyakhovsky[1], Y. Hamiel[1], P. Ampuero[2], Y. Ben-Zion[3]

1. Geological Survey of Israel, Jerusalem 95501, Israel (vladi@geos.gsi.gov.il)
2. Seismological Laboratory, California Institute of Technology (ampuero@gps.caltech.edu)
3. Department of Earth Sciences, University of Southern California Los Angeles, CA, 90089-0740, USA (benzion@usc.edu)

Submitted to *Geophys. J. Int.*, December 2008

In press, 2009

Summary

We address various deformational aspects of damaged materials with theoretical analyses and numerical simulations based on a nonlinear continuum damage model. Quasi-static simulations of damage accumulation under cyclic load reproduce the laboratory-observed increase in the difference between tensile and compressive elastic moduli with ongoing deformation beyond the elastic regime. Modeling of wave propagation effects reproduces the observed relations between the resonance frequency and wave amplitude. In agreement with laboratory experiments, the simulated resonant curves are asymmetric, with gradual decrease of wave amplitudes for frequencies higher than the resonance value and strong reduction for lower frequencies. The predicted shift of the resonance frequency with increasing wave amplitude under constant material damage is only a few percent, while the resonance frequency shift associated with increasing material damage may reach tens of percent. The results show that the employed continuum damage rheology model provides a self-consistent treatment for multiple manifestations of nonlinear elastic and brittle deformation of solids.

Keywords: Geomechanics, Elasticity and anelasticity, Fault zone rheology, Dynamics and mechanics of faulting, Seismic attenuation, Wave propagation.

1. Introduction

Rocks are generally considered as isotropic and linear elastic media. Linear elasticity leads to useful solutions for small strain deformation and provides a well-grounded basis for many practical applications. However, rock damage in the form of cracks, joints and other internal flaws can produce significant deviations from linear isotropic elasticity. The rock damage can grow with increasing stress and may affect profoundly the elastic moduli especially just before macroscopic failure (e.g., Lockner & Byerlee, 1980; Lockner *et al*., 1992; Hamiel *et al*., 2004). Experimental studies have documented various manifestations of nonlinear elasticity in rocks and rock-like materials (e.g., Nishihara, 1957; Brace, 1965; Zoback & Byerlee, 1975; Brady, 1969; Schock, 1977; Collins, 1981; Ambartsumyan, 1982; Alm *et al.*, 1985; Schmitt & Zoback, 1992; Weinberger *et al*., 1994; Johnson *et al*., 1996; Lockner & Stanchits, 2002; Hamiel *et al.* 2005). Nonlinear elasticity is also observed in seismic records of ground motion in sediments and highly-damaged fault zone rocks (e.g., Field *et al.*, 1997; Rubinstein & Beroza, 2004; Pavlenko & Irikura, 2003; Karabulut & Bouchon, 2007; Wu *et al*., 2009). Comparison of seismograms from weak and strong earthquakes indicates that attenuation becomes nonlinear at high amplitudes (e.g., Frankel *et al.*, 2002; Beresnev, 2002; Hatzell *et al.*, 2002, 2004; Bonilla *et al.*, 2005; Tsuda *et al.*, 2006, Sleep & Hagin, 2008).

Several studies pointed out that the values of the elastic moduli of damaged rocks change strongly when the loading reverses from compression to tension. For example, the Young modulus of graphite is 20% less under tension than it is under compression (Jones, 1977), the difference between the tensile and compressive Young moduli for different types of iron is up to 30%, and the compressive modulus for concrete may be (Ambartsumyan, 1982) up to three times larger then the tensile value. Walsh (1965) showed that the Young modulus of a cracked solid gradually increases with increasing uniaxial compression and related the material strengthening to crack closure under compressive stress. Basaran & Nie (2004) presented results of strain-controlled tension-compression uniaxial tests on a composite brittle material (lightly cross-linked poly-methyl methacrylate filled with alumina trihydrate) that show clear correlation between increasing crack density and decreasing stiffness. Their results (Fig. 1) explicitly demonstrate a gradual decrease of the tensile Young modulus as a function of the number of loading cycles, while the compressive modulus remains about constant. A comparison of these experimental observations with theoretical results based on a nonlinear continuum damage model is discussed in section 3.

Another manifestation of nonlinear elastic behavior in rocks was reported by several authors who analyzed a set of resonant bar experiments with rock samples (e.g., Gordon & Davis, 1968; Winkler *et al.*, 1979; Johnson *et al.*, 1996; Guyer *et al.*, 1999; Smith & TenCate, 2000; Pasqualini *et al.*, 2007). Instead of the constant resonant frequency expected for linear elastic media, increased external forcing was shown to produce a shift of the spectral peak to lower frequencies and asymmetric shape of the resonance curves (Fig. 2a). The experimental results indicate that the resonant frequency is constant at very low strains but starts to change and decreases linearly at intermediate strains (Fig. 2b). At larger strains corresponding in the lab experiments to accelerations above about 450 m/s^2, the frequency deviates from linear reduction and approaches a new constant value. The overall observed frequency shift in experiments with Lavoux sandstone (Fig. 2) and other rocks is of the order of a few percent. Several studies simulated a frequency shift at relatively low strains using a model that combines higher order terms in the free energy of a solid with an additional non-analytic term depending on both the strain and strain rate (e.g., Guyer *et al.*, 1997; Guyer & Johnson, 1999; Guyer *et al.*, 1999). Their model represents the bond system of a rock as an assemblage of hysteretic elastic elements that can only be in one of two states, open or closed. The existence of these elements forms cusps in the hysteresis loop (discrete memory) and also predicts cusps in low-amplitude stress-strain curves. Pasqualini *et al.* (2007) criticized this model and argued that there is no experimental evidence for cusp behavior in low-amplitude stress-strain loops. They also showed that predictions of a simple Duffing oscillator with a cubic term are consistent (see also TenCate *et al.*, 2004) with the data obtained at strains below a certain threshold.

Geotechnical analyses of seismic site response in soil and weak sediment deposits are usually carried out with equivalent-linear approximation of nonlinear stress-strain response. This empirical approach adopts the Kelvin-Voigt model and assumes in agreement with observations that both the effective shear modulus and seismic quality factor decrease with increasing shear strain (e.g., Seed & Idriss, 1970; Hardin &

Drnevitch, 1972; Sun *et al.*, 1988; Vucetic & Dobry, 1991). The equivalent-linear approximation approach accounts for resonance frequency shift and is the basis for many numerical codes for seismic site response that attempt to account for nonlinear elasticity (e.g., Schnabel *et al.,* 1972; Bardet *et al,* 2000; Assimaki & Kausel, 2002). Recently, Wu *et al.* (2009) observed strong temporal changes of the resonance frequency and motion amplification at a site on the North Anatolian fault with damaged fault zone rocks. They reproduced these observations using a model consisting of a low velocity fault zone layer in elastic half-space and the equivalent linear approximation for sets of material properties at different times. However, these and related simulations with the equivalent-linear approximation do not account for the evolution of the effective elastic properties with the ongoing deformation.

In the present paper we provide theoretical developments based on a nonlinear continuum model with a scalar damage state variable that is capable of accounting for evolving elastic moduli and attenuation coefficient during a damage process, along with nonlinear elasticity and wave propagation effects. The model is used to reproduce key nonlinear features of resonance curves observed in laboratory experiments with rocks that do not contain internal interfaces with impedance contrast. We apply a quasi-static modeling approach to simulate a damage accumulation process during brittle deformation that accounts explicitly for different moduli under tension and compression (e.g., *Basaran and Nie*, 2004), and wave propagation modeling to analyze the associated changes in the peak and shape of resonance frequency in rocks (e.g., Pasqualini *et al.,* 2007). The ability of the employed nonlinear damage model to account simultaneously for the evolution of multiple variables and response functions provides a strong test of its validity for describing realistic behavior of rocks.

2. Theory

The nonlinear continuum damage mechanics employed in this study models the effect of distributed cracks in terms of a single scalar damage state variable. Representative elementary volumes with a sufficiently large number of cracks corresponding to given values of the damage variable are assumed to be uniform and isotropic. A similar approach was used earlier in a linear continuum damage model (Kachanov, 1986) with a scalar damage parameter D defined as:

$$D = 1 - \frac{E}{E_0}, \tag{1}$$

where E is the instantaneous elastic modulus and E_0 is the initial undamaged value. Values of such a damage parameter were determined experimentally by Basaran & Nie (2004) and compared with their thermodynamically-based damage evolution function. In this approach, material with fixed damage (D=*const.*) remains linear with the same Young modulus under tension and compression. Predictions of the linear continuum damage models fit well tensile cycles of loading (Fig. 3), but show significant disagreement for material behavior under compression.

The experimentally observed stress-strain behavior (Fig. 1) may be represented as a bi-linear response with a constant Young modulus under compression and gradually degrading modulus under tensile loading (Fig. 4). Ignoring at this stage for mathematical simplicity the hysteresis effects, the associated one-dimensional stress-strain response can be written as:

$$\sigma = \begin{cases} E_0 \varepsilon & \text{for} \quad \varepsilon < 0 \\ E_0 (1-\alpha)\varepsilon & \text{for} \quad \varepsilon > 0 \end{cases}, \tag{2}$$

where σ is stress, E_0 is Young modulus of the linear elastic material, ε is elastic strain positive in tension, and $0 \leq \alpha \leq 1$ is a damage state variable. For $\alpha=0$ the material is linear elastic, while for $\alpha \rightarrow 1$ it is strongly nonlinear with a tensile Young modulus approaching zero. Equation (2) may be re-written using the absolute value of strain:

$$\sigma = E_0 \left(\left(1 - \frac{\alpha}{2} \right) \varepsilon - \frac{\alpha}{2} |\varepsilon| \right). \tag{3}$$

Figure 4 schematically represents evolving one-dimensional stress-strain curves starting with an intact rock. The tensional modulus decreases with damage increase and approaches zero at the macroscopic failure.

The variations of Young modulus and Poisson ratio with damage intensity under different types of load in three dimensions can be described (e.g., Lyakhovsky *et al.,* 1997a, 1997b) by extending the free energy of the elastic solid to the form:

$$U = \frac{1}{\rho}\left(\frac{\lambda}{2}I_1^2 + \mu I_2 - \gamma I_1\sqrt{I_2}\right), \tag{4}$$

where $I_1=\varepsilon_{ii}$ and $I_2=\varepsilon_{ij}\varepsilon_{ij}$ are the first and second invariants of the elastic strain tensor and ρ is the mass density. The elastic energy potential (4) includes two quadratic Hookean terms of the elastic strain tensor ε_{ij} associated with the Lamé moduli λ and μ, and an additional nonlinear second order term associated with a third modulus γ. The first two terms of (4) give the classical strain potential of linear elasticity. The third term may be derived using the effective medium theory of Budiansky & O'Connell (1976) for non-interacting cracks that dilate and contract in response to tension and compression (Lyakhovsky *et al.,* 1997b), or by expanding the strain energy potential as a general second-order function of I_1 and I_2 and eliminating non-physical terms (Ben-Zion & Lyakhovsky, 2006). Differentiation of the elastic energy (4) with respect to the strain tensor ε_{ij} leads to a constitutive stress-strain ($\sigma_{ij} - \varepsilon_{ij}$) relation of the form

$$\sigma_{ij} = \rho\frac{\partial U}{\partial \varepsilon_{ij}} = \left(\lambda - \frac{\gamma}{\xi}\right)I_1\delta_{ij} + 2\left(\mu - \frac{1}{2}\gamma\xi\right)\varepsilon_{ij}, \tag{5}$$

where δ_{ij} is Kronecker delta and $\xi = I_1/\sqrt{I_2}$. The variable ξ is referred to as the strain invariants ratio and it ranges from $\xi = -\sqrt{3}$ for isotropic compaction to $\xi = +\sqrt{3}$ for isotropic dilation. Equation (5) reduces to linear Hookean elasticity for an undamaged solid (γ=0). The cumulative effect of distributed micro-cracks and flaws in the elastic material leads to reduction of the effective elastic moduli and nonlinear elasticity with asymmetric response to loading under tension and compression conditions. The stress-strain relations (5) with nonzero γ are reduced in a one-dimensional case to the bi-linear relation (2) or (3).

During ongoing deformation the elastic moduli in (4) and (5) may degrade if the stress-strain conditions are above a yielding threshold $\xi \geq \xi_0$. This is accounted for by making the elastic moduli functions of a scalar damage state variable and deriving a kinetic equation for the evolution of α (e.g., Lyakhovsky & Myasnikov, 1984, 1985; Agnon & Lyakhovsky, 1995; Lyakhovsky *et al.,* 1997a,b). Using the balance equations of energy and entropy, the entropy production density is represented as a product of a thermodynamic flux and a thermodynamic force $(d\alpha/dt)\times(\partial U/\partial\alpha)$. Adopting the Onsager (1931) principle of linear relations between thermodynamic forces and fluxes, the equation of damage evolution has the form (Lyakhovsky *et al.,* 1997a):

$$\frac{d\alpha}{dt} = -C\frac{\partial U}{\partial \alpha}, \tag{6a}$$

where *C* is a positive function of state variables that ensures non-negative local entropy production. Assuming for simplicity that the moduli μ and γ are linear functions of α and that λ is constant, and using in (6a) the potential (4), leads to the following evolution equation during material degradation:

$$\frac{d\alpha}{dt} = C_d I_2(\xi - \xi_0) \ \ for \ \ \xi \geq \xi_0. \tag{6b}$$

The coefficient C_d gives the rate of positive damage evolution (material degradation) for $\xi > \xi_0$ and may be constrained by laboratory fracturing experiments (e.g., Lyakhovsky *et al*, 1997a; Hamiel *et al*, 2004). The rate of damage recovery (material healing) is not relevant for this study, but can be incorporated in the model formulations (e.g., Lyakhovsky *et al*, 1997a; 2005). Following the onset of positive damage evolution above the elastic limit at $\xi = \xi_0$, and before the final macroscopic failure, the model incorporates a gradual accumulation of inelastic strain, ε_{ij}^{i}, given by (Hamiel *et al*, 2004):

$$\frac{d\varepsilon_{ij}^{i}}{dt} = C_v \frac{d\alpha}{dt} \tau_{ij}, \tag{7}$$

where C_v is a material constant and $\tau_{ij} = \sigma_{ij} - \sigma_{kk}\delta_{ij}/3$ is the deviatoric stress tensor. The damage-related compliance or inverse of viscosity (C_v dα/dt) relates the deviatoric stress to the rate of gradual irreversible strain accumulation. As in Maxwell visco-elasticity, the total strain tensor, $\varepsilon_{ij}^{t} = \varepsilon_{ij} + \varepsilon_{ij}^{i}$, is a sum of the elastic strain tensor and the irreversible viscous component of deformation. This implies that the amount of irreversible strain that accumulates before the final macroscopic failure is proportional to the overall damage increase in the rock volume. Additional details on the damage model in relation to laboratory experiments and phenomenology of earthquakes and faults can be found in Lyakhovsky & Ben-Zion (2008) and Ben-Zion (2008). Damage models for slow large-scale geophysical applications are discussed by, e.g., Bercovici & Ricard (2003), Hobbs *et al* (2008) and Ricard & Bercovici (2009).

3. Modeling results

3.1. Quasi-static damage evolution

The bi-linear behavior in equations 2 or 3 (see also Fig. 4) clearly describes a decrease of the effective modulus for tension with increasing damage. Therefore it allows a significantly improved fitting between results of the nonlinear damage rheology and the experimental data shown in Figure 3 (Basaran & Nie, 2004). Values of the damage parameters should change from α~0.15 for cycle #5, to 0.2 for cycle #50, and up to α~0.25 for the last reported cycle #104. This damage increase with the reported strain values constrains the damage rate coefficient to be C_d~10^2 s^{-1}. Accounting for the gradual accumulation of inelastic strain (7) with C_V~10^{-7} Pa^{-1} reproduces the hysteresis observed in the experiment during the various cycles. A more precise calibration of the model parameters, of the type done previously by Hamiel *et al*. (2004, 2006), requires detailed measurements of the sample deformation under different loading conditions which are not available for this test. However, such calibration is not essential for the present work concerned with general nonlinear wave-propagation aspects of damaged rocks.

3.2. Wave resonance

3.2.1. 1-D case

In this section we present a one-dimensional model of the resonance frequency shift in a nonlinear material. First we derive two analytical end-member solutions for small and large wave amplitudes. In order to account for attenuation, the one-dimensional bi-linear stress-strain relation (3) is generalized, following Kelvin-Voigt rheology, to the form:

$$\sigma = E_0\left(\left(1-\frac{\alpha}{2}\right)\varepsilon - \frac{\alpha}{2}|\varepsilon| + \eta\dot{\varepsilon}\right), \tag{8}$$

where η is the viscosity divided by Young modulus. Expressing the elastic strain, ε, as a derivative of the displacement vector u $(\varepsilon = \partial u/\partial x)$, the equation of motion for a forced oscillator with Kelvin-Voigt damping can be written as

$$E_0\left[\left(1-\frac{\alpha}{2}\right)\frac{\partial^2 u}{\partial x^2} - \frac{\alpha}{2}\frac{\partial}{\partial x}\left|\frac{\partial u}{\partial x}\right| + \eta\frac{\partial}{\partial t}\frac{\partial^2 u}{\partial x^2}\right] - \rho\frac{\partial^2 u}{\partial t^2} = F_{ext}\,, \tag{9}$$

where F_{ext} is the external forcing. For periodic forcing with frequency ω, the amplitude of the generated standing wave is maximal at the resonance frequency, which in the linear case does not depend on the amplitude of the wave itself. Eq. (9) for a damage-free material (α=0) becomes linear and predicts a constant resonance frequency $\omega_0^2 = E_0\kappa^2/\rho$, which depends on the material properties, E_0, ρ, and wave number κ of the standing wave that is related to the sample length. The complex wave amplitude,

$A(\omega)$, depends on the amplitude of the applied forcing, σ_0, material properties and quality factor $Q = 1/\eta\omega$ of the solid as:

$$A(\omega) = \frac{\sigma_0}{E_0 k\left[\left(\frac{\omega^2}{\omega_0^2} - 1\right) - \frac{i}{Q}\right]}. \tag{10}$$

For a damaged material ($\alpha>0$), the stress-strain relations are nonlinear and pre-existing strain (or stress) significantly changes the material behavior. We assume that the elastic strain, ε, is a sum of some pre-existing reference strain, ε_0, and additional strain related to the wave propagation, $\varepsilon = \varepsilon_0 + \partial u/\partial x$. With this notation, the term $\partial u/\partial x$ in (9) should be substituted by $\varepsilon_0 + \partial u/\partial x$. In the case of small wave amplitude, $|\partial u/\partial x| < |\varepsilon_0|$, the nonlinear term $|\varepsilon_0 + \partial u/\partial x| = -(\varepsilon_0 + \partial u/\partial x)$ for compressive pre-existing strain $(\varepsilon_0 < 0)$. This assumption eliminates the nonlinearity of the wave equation (9) and the solution coincides with the linear case (10). For a large wave amplitude $(|\partial u/\partial x| >> |\varepsilon_0|)$, the pre-existing strain may be neglected. We search for a solution of equation (9) with periodic forcing in the form of Fourier series. It should be noted that the second nonlinear term $(\partial/\partial x|\partial u/\partial x|)$ in equation (9) does not contribute to the first harmonic, but transfers the energy of the oscillations to higher harmonics. The amplitude of the first harmonic, $A_1(\omega)$, is:

$$A_1(\omega) = \frac{\sigma_0}{E_0\left(1 - \frac{\alpha}{2}\right)k\left[\left(\frac{\omega^2}{\left(1 - \frac{\alpha}{2}\right)\omega_0^2} - 1\right) - \frac{i}{Q\left(1 - \frac{\alpha}{2}\right)}\right]}. \tag{11}$$

This solution shows a reduction of the resonance frequency of high amplitude oscillations with increase of the material damage:

$$\omega_{res} = \sqrt{1 - \frac{\alpha}{2}}\omega_0 . \tag{12}$$

The two end-members amplitude-frequency relations for small (10) and large (11) amplitude oscillations demonstrate the general tendency for a shift of the resonance frequency with increasing amplitude of the wave.

3.2.2. 2-D case

An analysis of the entire shape of the resonance curve and its evolution with forcing amplitude and level of material damage requires a numerical study. To model the resonance frequency in a two-dimensional nonlinear material (eq. 5), we simulate wave propagation by discretizing the space domain with a spectral element method and the time domain with a finite difference scheme (Appendix A). Figure 5 presents simulated curves of wave amplitude versus forced frequency and various forcing amplitudes (numbers above the curves). The simulations are done in a spatial domain of size 200x1000 m^2 with a vertical size equal to 1/4 of the wave length (V_p=4000 m/s, f=1 Hz). The used viscosity parameter η=8 10^{-4} s corresponds to a quality factor Q=200 for 1 Hz $\left(Q(f) = 1/2\pi f\eta\right)$ and the source operates at the top edge. The bottom edge is fixed (zero displacement) and free-slip conditions are applied at the vertical edges. After a transient period, a standing wave with constant amplitude is formed in the simulated area.

The first set of simulations was done for a material with damage value α=0.3 and initial compaction ε_0=10^{-6}. For small forcing lower than 100 Pa (Fig. 5), the wave-induced deformation is below the initial compaction and the resonance curve is approximately linear and symmetric. With increasing forcing and wave-induced deformation, the maximum amplitude corresponding to the resonance frequency shifts to lower values and the entire curve becomes very asymmetric. The wave amplitude decreases gradually for frequencies higher than the resonance value, but decreases abruptly for lower frequencies. A similar asymmetry is observed in the laboratory experiment with Lavoux sandstone (Fig. 2a). With further increase of the forcing amplitude, the resonance frequency approaches a constant value in agreement with the experimental observations (Fig. 2b) and prediction of the analytical model. Figure 6a with logarithmic scale of the forcing axis illustrates the frequency change at low values of forcing, while Figure 6b with linear scale illustrates the behavior at large forcing. As evident from eq. (10), in a linear system the wave amplitude at the resonance frequency, $A_{res} = Q\sigma_0 / E_0 k$, depends on the quality factor and is proportional to the applied forcing. For the simulated nonlinear system this proportionality holds only for small forcing values (Fig. 7). For forcing larger than some threshold value, which depends on the damage level and initial strain ε_0, the wave amplitude increases less than expected for the linear system. Energy transfer from the resonance frequency to higher harmonics in the nonlinear system provides additional damping mechanism without changing the viscosity parameter of the Kelvin-Voigt model. The effective quality factor, which is defined as the ratio between wave amplitude and the applied forcing, decreases. However, for very large forcing, when the resonance frequency approaches its constant asymptotic value, the wave amplitude becomes proportional to the forcing value with the same coefficient of proportionality, as expected from eq. (11).

The results of the simulations discussed so far demonstrate explicitly nonlinear effects in damaged material with fixed properties. A resonance frequency shift may also be generated by temporal changes of the level of rock damage. An accumulation of damage in rocks leads to reduction of the effective elastic moduli and associated decrease of the seismic wave velocity, along with damage- and stress-induced anisotropy under non-hydrostatic load (e.g., Hamiel *et al*., 2009). Figure 8 presents two sets of simulated resonance curves for material with different levels of damage under small 100 Pa (Fig. 8a) and large 10,000 Pa (Fig. 8b) forcing. The material damage varies from α=0 for a damage-free solid to α=0.6. The latter is close to a critical damage level for the applied stress field, which consists of 1 MPa vertical compaction (corresponding to several tens of meters depth) and horizontal shearing with principle stresses of 2 MPa in one direction and zero in the other. Under these conditions the shift of the resonance frequency for vertically propagating wave is mostly controlled by the damage-related reduction in the effective elastic moduli and only slightly affected by the increased forcing. With a constant viscosity parameter of the Kelvin-Voigt model and small amplitude loading (Fig. 8a), the resonance frequency goes down with increasing damage from 1 Hz to below 0.7 Hz. In this case the shape of the resonance curves remains symmetric and the resonance amplitude increases, as expected for a linear system with frequency-dependent quality factor. A similar shift of the resonance frequency is obtained for large amplitude forcing (Fig. 8b), but the nonlinear effects produce a reduction of the resonance amplitude. This demonstrates again that nonlinear rheology leads to a decrease of the effective quality factor of the media. The amplitude-related shift and asymmetry of the resonance curve are not very pronounced but may be recognized by focusing on the small frequency range 0.6-0.75 Hz for the simulations with α=0.6 (Fig. 8c). The results predict that a highly damaged rock has resonance frequency lower than that of an intact rock, and that its quality factor is significantly reduced for large amplitude oscillations.

4. Discussion

We present theoretical results and numerical simulations of slow deformation and wave propagation effects in materials governed by a nonlinear damage rheology model, and compare the results with two sets of laboratory experiments. Strain-controlled tension-compression uniaxial tests (Basaran & Nie, 2004) explicitly demonstrate changes of the elastic moduli of brittle solid with stress reversal from tension to compression, together with gradual material degradation during cyclic load. Another set of experiments with rock samples (e.g., Gordon & Davis, 1968; Winkler *et al.*, 1979; Johnson *et al.*, 1996; Guyer *et al.*, 1999; Smith & TenCate, 2000; Pasqualini *et al.*, 2007) demonstrate shifts of the spectral peak to lower frequencies with increased external forcing. Instead of the symmetric bell-shaped resonant curve expected for linear elastic media, they recorded asymmetric shapes with a gradual decrease of wave amplitude for frequencies higher than the resonance value and fast drop for lower frequencies. These two sets of experiments, and the additional laboratory and seismological observations mentioned in the introduction, illustrate different manifestations of nonlinear elastic behavior of brittle materials.

Several approached have been used to address nonlinear elastic behavior of material deformation. Nonlinear stress–strain relationships can be approximated by including higher-order terms of the strain tensor in the elastic energy expression (e.g., Murnaghan, 1951; Brugger, 1964). Such models can be successful in large strain analysis of the Earth's interior (e.g., Birch, 1952), but they are out of range for small elastic deformations. The nonlinear elastic moduli of the Murnaghan model estimated from stress-induced seismic anisotropy are three to four orders of magnitude higher then the Lame moduli and are not realistic in comparison to those obtained from static experiments (Johnson & Rasolofosaon, 1996). Following the Duffing model, introduced by TenCate *et al.* (2004), Pasqualini *et al*. (2007) added a quadratic term to the equation of motion for damped harmonic oscillator. However, their model failed to reproduce the frequency shift under relatively high strains. They argue that at high strains there is a transition to non-equilibrium dynamic state and that "theoretical framework which encompasses and explains all known physical effects needs to be developed". Sleep & Hagin (2008) discussed two nonlinear processes associated with strong seismic shaking, nonlinear increase in attenuation of strong seismic waves and effects of damage in the shallow subsurface. They suggested accounting for the energy dissipation related to the crack dilation as an attenuation mechanism, and proposed an explanation of nonlinear time-dependent wave propagation effects based on rate- and state-dependent friction.

Most of the employed approaches are successful in describing certain aspects of the observations while leaving out other features. In the present paper we attempt to provide a self-consistent explanation for various observed nonlinear features of deformation within a single approach based on a nonlinear continuum damage rheology. Previous studies with the model (Lyakhovsky *et al.,* 1997a, Hamiel *et al.,* 2005; Hamiel *et al*, 2006) demonstrated that the nonlinear stress–strain relations (5) derived from the elastic potential (4), reproduce change in the effective elastic moduli under stress reversal in a four-point beam test reported by Weinberger *et al.* (1994), rock dilation due to deviatoric stresses (Lockner & Stanchits, 2002), and stress-induced seismic wave anisotropy (Stanchits *et al.*, 2006). Recently Hamiel *et al.* (2009) analyzed laboratory fracturing experiments of granite sustaining several cycles of deformation. They constrained the parameters of the damage rheology model by the stress–strain relation measured during load cycles and calculated *P*-wave velocities including stress- and damage-induced seismic wave anisotropy. The simultaneous fit to both the strain–stress curves and the measured velocity values with the same set of model parameters demonstrate that the nonlinear damage model accounts for the different aspects of the stress–strain fields beyond linear elasticity.

Our quasi–static simulations of damage accumulation account for different moduli under tension and compression (Basaran & Nie, 2004), while the dynamic simulations of wave propagation reproduce the shift and asymmetries of the resonance frequency observed in different laboratory experiments. If the background stress has a zero deviatoric component, the model predicts bi-linear stress–strain relation with a kink at the transition from tension to compaction. In this case, which may represent some laboratory conditions (Fig. 2a), the resonance curve has a very sharp asymmetry (Fig. 5). For more realistic background stresses incorporating shear components, the transition from tension to compaction is smoothed and the peak of the resonance curve is more gradual (Fig. 8c). The analytical solution and numerical simulations predict a shift of the resonance frequency to lower values due to nonlinear effects. In agreement with the laboratory results, this shift is very small (only a few percent). However, the change of the elastic moduli and corresponding decrease of the seismic wave velocity due to material degradation (damage increase) may reach tens of percent (Fig. 8). This feature is consistent with in-situ seismological observations and may be reproduced by simulations with equivalent linear elastic model that employ different sets of material properties (e.g., Karabulut & Bouchon, 2007; Wu *et al.*, 2009). However, the nonlinear damage rheology of the present paper provides a more physical approach for treating such data.

The presented modeling results demonstrate that for small amplitudes the wave amplification is similar to that predicted by linear elasticity (Fig. 7). With increased amplitude the amplification becomes weaker, similarly to what is usually assumed in equivalent linear elastic model, but for very high amplitudes the amplification approaches values predicted by linear elasticity. This behavior is related to the laboratory measured response (Fig. 2b), as well as our analytical and numerical results (Fig. 6), that the resonance frequency approaches a constant value at very high amplitudes instead of a continuous shifting. Standard engineering calculations (e.g., Seed & Idriss, 1970) usually ignore this feature of the nonlinear elastic rock behavior and may thus underestimate the maximal amplitudes of strong ground shaking in highly damage materials.

Acknowledgments

We thank the editor Y. Ricard and two anonymous referees for constructive reviews. The studies were supported by grants from the Israel Science Foundation (ISF 753/08) and the Southern California Earthquake Center (based on NSF Cooperative Agreement EAR-0106924 and USGS Cooperative Agreement 02HQAG0008).

Appendix A: Spectral element method for nonlinear wave propagation.

The nonlinear wave propagation problem is solved by discretizing the space domain with a spectral element method (SEM) and the time domain with a finite difference scheme. The SEM is a high order method that shares the geometrical flexibility of the finite element method and the accuracy of spectral methods. In computational seismology this method is widely used for linear elastic wave propagation (*Komatitsch and Vilotte*, 1998; *Chaljub et al.*, 2007; *Komatitsch et al.*, 2005) and has been applied more recently in earthquake dynamics (*Madariaga et al.*, 2006; *Festa and Vilotte*, 2006). High order methods have been also succesfully applied to static elasto-plastic problems (*Holzer and Yosibashi*, 1996; *Düster and Rank*, 2002) and have been shown to conserve their accuracy on a range of nonlinear problems with sufficient smoothness.

The continuum damage rheology was implemented in the spectral element code SEM2DPACK (*Ampuero*, 2008), assuming two-dimensional, infinitesimal, plane strain deformation. Given the narrow frequency band distribution of the source, attenuation was modeled by a Kelvin-Voigt rheology. This amounts to replace in the constitutive equations the elastic strain ε by $\varepsilon^* = \varepsilon + \eta\dot{\varepsilon}$, where η is a viscosity parameter. In the linear problem, the resulting quality factor Q is frequency-dependent, $Q(\omega) = 1/\eta\omega$, and η is selected to achieve a given Q value at the dominant frequency of the source.

The domain is decomposed in quadrilateral elements, possibly deformed. Within each element, the kinematic fields are approximated as a tensor product of polynomials of order p. Each element is provided with a spectral subgrid of $(p+1)^2$ Gauss-Lobatto-Legendre nodes, which serve as both interpolation and quadrature nodes. Like in the finite element method, the spectral element discretization of the variational formulation of the governing equations leads to the algebraic system

$$Ma = F_{\text{int}}(d + \eta v) + F_{ext} . \tag{A1}$$

where M is a mass matrix, diagonal by construction (artificial mass lumping is not required), d, v and a are the nodal displacements, velocities and accelerations, respectively, F_{int} and F_{ext} are internal and external forces, respectively.

The time discretization is done with a centered (second-order) finite difference scheme, with time-staggered displacements and velocities. Denoting by a subscript *k* the quantities evaluated at time $t_k = k \cdot \Delta t$, the discrete equations are:

$$d_{k+1} = d_k + \Delta t \cdot v_{k+1/2} . \tag{A2}$$

$$\frac{v_{k+3/2} - v_{k+1/2}}{\Delta t} = F_{\text{int}}(d_{k+1} + \eta \cdot v_{k+1/2}) + F_{ext}(t_{k+1}). \tag{A3}$$

The evaluation of F_{int} is done through direct stiffness summation. The strains ε^*_{k+1} are evaluated from $d_{k+1} + \eta \cdot v_{k+1/2}$ at the element level, then stresses σ_{n+1} are updated from the constitutive equations, and finally the elementary contribution is assembled into the global internal forces F_{int}. Note that, for convenience, the velocity term in ε^* is evaluated with half time step delay.

References

Agnon, A. & Lyakhovsky, V., 1995. Damage distribution and localization during dyke intrusion, in: *The Physics and Chemistry of Dykes*, pp. 65-78, eds Baer G. & Heimann A., Balkema, Rotterdam.

Alm, O., Jaktlund, L.L. & Kou, S., 1985. The influence of microcrack density on the elastic and fracture mechanical properties of Stripa granite, *Phys. Earth planet. Inter*., 40, 161-179.

Ambartsumyan, S.A., 1982. *Raznomodulnaya Teoria Uprugosti (strain-dependence elastic theory)*, Nauka, Moscow (in Russian).

Ampuero, J.-P., 2008. SEM2DPACK, A Spectral Element Method tools for 2D wave propagation and earthquake source dynamics, User's Guide, version 2.3.0. Available online at http://www.sourceforge.net/projects/sem2d/.

Assimaki, D. & Kausel, E., 2002. An equivalent linear algorithm with frequency- and pressure-dependent moduli and damping for the seismic analysis of deep sites. *Soil Dynamics and Earthquake Engineering*. 22, 959–965.

Bardet, J.P., Ichii, K. & Lin, C.H., 2000. *EERA – A computer program for Equivalent-linear Earthquake site Response Analyses of Layered Soil Deposits*. University of Southern California, Department of Civil Engineering.

Basaran C. & Nie, S., 2004. An irreversible thermodynamics theory for damage mechanics of solids. *Int. J. Damage Mach.* 13, 205-223.

Ben-Zion, Y., 2008. Collective Behavior of Earthquakes and Faults: Continuum-Discrete Transitions, Evolutionary Changes and Corresponding Dynamic Regimes, *Rev. Geophysics*, 46, RG4006, doi:10.1029/2008RG000260.

Ben-Zion, Y. & Lyakhovsky, V., 2006. Analysis of aftershocks in a lithospheric model with seismogenic zone governed by damage rheology, *Geophys. J. Int*., 165, 197-210.

Bercovici, D. and Ricard, Y., 2003. Energetics of a two-phase model of lithospheric damage, shear localization and plate boundary formation, *Geophys. J. Int.*, 152, 581–596.

Beresnev, I.A., (2002). Nonlinearity at California generic soil sites from modeling recent strong-motion data. *Bull. Seismol. Soc. Am.*, 92,863-870, doi:10.1785/0120000263.

Birch, F., 1952. Elasticity and constitution of the Earth's interior, *J. Geophys. Res*, 57, 221-286.

Bonilla, L.F., Archuletta, R.J. and Lavallee, D., 2005. Hysteretic and dilatant behavior of cohesionless soils and their effects on nonlinear site response: Field data observations and modeling. *Bull. Seismol. Soc. Am.*, 95, 2273-2395, doi 10.1785/0120040128.

Brace, W.F., 1965. Some new measurements of the linear compressibility of rocks, *J. Geophys. Res.* 70, 391–398.

Brady, B.T., 1969. The non-linear behavior of brittle rock, *Int. J. Rock Mech. Min. Sci. Geomech. Abstr.* 6, 301– 310.

Budiansky, B., & O'Connell, R.J., 1976. Elastic moduli of a cracked solid. *Int. J. Solids Struct.*, 12, 81-97.

Brugger, K., 1964. Thermodynamic definition of higher order elastic constants, *Phys. Rev.* 133, 1611 –1612.

Chaljub, E., Komatitsch, D., Vilotte, J.P., Capdeville, Y., Valette, B., & Festa, G., 2007. Spectral element analysis in seismology, in: *Advances in wave propagation in heterogeneous media*, *Volume 48 of Advances in Geophysics*, pp. 365–419, eds Wu, R.-S. & Maupin, V., Elsevier, Academic Press.

Collins, J.A., 1981. *Failure of Materials in Mechanical Design*, Wiley, New York, NY.

Düster, A., & Rank, E., 2002. A p-version finite element approach for two- and three-dimensional problems of the J2 flow theory with non-linear isotropic hardening. *Int. J. Numer. Meth. Engng.*, 53, 49–63

Festa, G., & Vilotte, J.-P., 2006. Influence of the rupture initiation on the intersonic transition: Crack-like versus pulse-like modes. *Geophys. Res. Lett.* 33, L15320, doi:10.1029/2006GL026378.

Field, E.H., Johnson, P.A., Beresnev, I.A. & Zeng, Y., 1997. Nonlinear ground-motion amplification by sediments during the 1994 Northridge earthquake, *Nature*, 390, 599–602.

Frankel, A.D., Carver, D.L., & Williams, R.A., 2002. Non-linear and linear site response and basin effects in Seattle for the M 6.8 Nisqually, Washington, earthquake. *Bull. Seismol. Soc. Am.*, 92, 2090–2109. doi:10.1785/0120010254

Gordon, R. B., & Davis, L. A., 1968. Velocity and attenuation of seismic waves in imperfectly elastic rocks, *J. Geophys. Res.*, 73, 3917–3935.

Guyer, R. A., & Johnson, P. A., 1999. Nonlinear mesoscopic elasticity, evidence for a new class of materials, *Phys. Today*, 52, 30–35.

Guyer, R. A., TenCate, J., & Johnson, P. A., 1999. Hysteresis and the dynamic elasticity of consolidated granular materials, *Phys. Rev. Lett.*, 82, 3280–3283.

Guyer, R. A., McCall, K. R., Boitnott, G. N., Hilbert Jr., L. B., & Plona, T. J., 1997. Quantitative implementation of Preisach-Mayergoyz space to find static and dynamic elastic moduli in rock, *J. Geophys. Res.*, 102, 5281–5293.

Hamiel, Y., Liu, Y., Lyakhovsky, V., Ben-Zion, Y. & Lockner, D., 2004. A visco-elastic damage model with applications to stable and unstable fracturing, *Geophys. J. Int.*, 159, 1155−1165.

Hamiel, Y., Lyakhovsky, V. & Agnon, A., 2005. Rock dilation, Nonlinear deformation, and pore pressure change under shear, *Earth Plan. Sci. Lett.*, 237, 577−589.

Hamiel, Y., Katz, O., Lyakhovsky, V., Reches, Z., & Fialko Y., 2006. Stable and unstable damage evolution in rocks with implications to fracturing of granite. *Geophys. J. Int.*, 167, 1005−1016.

Hamiel, Y. Lyakhovsky, V., Stanchits, S., Dresen, G. & Ben-Zion, Y. 2009. Brittle deformation and damage-induced seismic wave anisotropy in rocks. *Geophys. J. Int.*, (in press).

Hardin, B. O. & Drnevich, V. P., 1972. Shear Modulus and Damping in Soils: II. Design Equations and Curves. *J. Soil Mechanics Foundation Division, ASCE,* 98, 667−691.

Hatzell, S., Leeds, A., Frankel, A., Williams, R.A., Odum, J., Stephenson, W., & Silva, W., 2002. Simulation of brad-band ground motion including nonlinear soil effects for a magnitude 6.5 earthquake on the Seattle fault, Seattle, Washington. *Bull. Seismol. Soc. Am.*, 92, 831−853, doi:10.1785/0120010114.

Hatzell, S., Bonilla, L.F., & Williams, R.A., 2004. Prediction of nonlinear soil effects, *Bull. Seismol. Soc. Am.*, 94, 1609–1629, doi:10.1785/012003256.

Hobbs, B., Regenauer-Lieb, K. & Ord, A., 2008. Folding with thermal–mechanical feedback, *J. Struct. Geol.*, 30, 1572–1592.

Holzer, S. M., & Yosibashi, Z., 1996. The p-version of the finite element method in incremental elasto-plastic analysis, *Int. J. Numer. Meth. Engng.*, 39, 1859–1878.

Johnson, P.A., & Rasolofosaon, P.N.J., 1996. Nonlinear elasticity and stress-induced anisotropy in rock, *J. Geophys. Res*. 101, 3113–3124.

Johnson, P. A., & Jia, X., 2005. Nonlinear dynamics, granular media and dynamic earthquake triggering, *Nature*, 473, 871–874.

Johnson, P.A., Zinszner, B. & Rasolofosaon, P.N.J., 1996. Resonance and elastic nonlinear phenomena in rock, *J. Geophys. Res*. 101, 11553–11564.

Kachanov, L.M., 1986. *Introduction to Continuum Damage Mechanics*, Martinus Nijhoff Publishers, 135 p.

Karabulut, H., & Bouchon, M., 2007. Spatial variability and non-linearity of strong ground motion near a fault, *Geophys. J. Int.,* 170, 262–274, doi:10.1111/j.1365-246X.2007.03406.x.

Komatitsch, D., & Vilotte, J. P., 1998. The spectral element method: an efficient tool to simulate the seismic response of 2D and 3D geological structures. *Bull. Seism. Soc. Am*. 88, 368–392.

Komatitsch, D., Tsuboi, S., & Tromp, J., 2005. The spectral element method in seismology, in: *Seismic Earth: Array Analysis of Broadband Seismograms,* pp. 205–228, eds Levander, A., & Nolet, G., Volume 157 of Geophysical Monograph. Washington DC, USA, American Geophysical Union.

Lockner, D. A., Byerlee, J.D., Kuksenko, V., Ponomarev, A., & Sidorin, A., 1992. Observations of quasi-static fault growth from acoustic emissions, in: *Fault mechanics and transport properties of rocks, International Geophysics Series, Vol. 51*, p. 3–31, eds Evans, B. & Wong, T.-f., Academic Press, San Diego, CA.

Lockner, D.A., & Byerlee, J.D., 1980. Development of fracture planes during creep in granite, in: *2nd Conference on Acoustic Emission/Microseismic Activity in*

Geological Structures and Materials, pp. 1 –25, eds Hardy, H.R., & Leighton, F.W., Trans-Tech. Publications, Clausthal-Zellerfeld, Germany.

Lockner, D.A., & Stanchits, S.A., 2002. Undrained poroelastic response of sandstones to deviatoric stress change, *J. Geophys. Res.* 107, doi:10.1029/2001JB001460.

Lyakhovsky, V., & Ben-Zion, Y., 2008. Scaling relations of earthquakes and aseismic deformation in a damage rheology model, *Geophys. J. Int.*, 172**,** 651−662, doi: 10.1111/j.1365-246X.2007.03652.x.

Lyakhovsky, V., & Myasnikov, V.P., 1984. On the behavior of elastic cracked solid, *Phys. Solid Earth*, 10, 71−75 .

Lyakhovsky, V., & Myasnikov, V.P., 1985. On the behavior of visco-elastic cracked solid, *Phys. Solid Earth*, 4, 28−35.

Lyakhovsky, V., Ben-Zion, Y. & Agnon, A., 1997a. Distributed damage, faulting, and friction, *J. Geophys. Res.*, 102, 27,635−27,649.

Lyakhovsky, V., Reches, Z., Weinberger, R., & Scott, T.E., 1997b. Non-linear elastic behavior of damaged rocks, *Geophys. J. Int.*, 130, 157−166.

Madariaga, R., Ampuero, J.-P., & Adda-Bedia, M., 2006. Seismic radiation from simple models of earthquakes, in: *Earthquakes: Radiated Energy and the Physics of Earthquake Faulting*, pp. 223–236, eds McGarr, A., Abercrombie, R., Kanamori, H., & di Toro, G., Volume 170 of Geophysical Monograph, Am. Geophys. Union.

Murnaghan, F.D., 1951. *Finite Deformation of an Elastic Solid*, John Wiley, Chapman, New York, 140 pp.

Nishihara, M., 1957. Stress–strain relation of rocks, *Doshisha Eng. Rev*. 8, 32–54.

Onsager, L., 1931. Reciprocal relations in irreversible processes. *Phys. Rev*., 37, 405–416.

Pasqualini, D., Heitmann, K., TenCate, J.A., Habib, S., Higdon, D., & Johnson, P.A., 2007. Nonequilibrium and nonlinear dynamics in Berea and Fontainebleau sandstones: Low-strain regime. *J. Geophys. Res*., 112, B01204, doi:10.1029/2006JB004264.

Pavlenko, O.V., & Irikura, K., 2003. Estimation of nonlinear time-dependent soil behavior in strong ground motion based on vertical array data, *Pure Appl. Geophys.,* 160**,** 2365-2379.

Ricard, Y. & Bercovici, D, 2009, A continuum theory of grain size evolution and damage, *J. Geophys. Res.*, 114, B01204, doi:10.1029/2007JB005491.

Rubinstein, J.L., & Beroza, G.C., 2004. Evidence for Widespread Nonlinear Strong Ground Motion in the Mw 6.9 Loma Prieta Earthquake, *Bull. Seism. Soc. Am.,* 94, 1595−1608.

Schmitt, D.R., & Zoback, M.D., 1992. Diminished pore pressure in low-porosity crystalline rock under tensional failure: apparent strengthening by dilatancy, *J. Geophys. Res.* 97, 273–288.

Schnabel, P. B., Lysmer, J., & Seed, H. B., 1972. SHAKE: A Computer Program for Earthquake Response Analysis of Horizontally Layered Sites, Report No. UCB/EERC-72/12, Earthquake Engineering Research Center, University of California, Berkeley, December, 102p.

Schock, R.N., 1977. The response of rocks to large stresses, in: *Impact and Explosion Cratering*, pp. 657–688, eds Roddy, D.L., Pepin, R.O., & Merrill, R.B., Pergamon Press, New York.

Seed, H. B., & Idriss, I. M., 1970. Soil Moduli and Damping Factors for Dynamic Response Analysis, Report No. UCB/EERC-70/10, Earthquake Engineering Research Center, University of California, Berkeley, 48p.

Sleep, N. H., & Hagin P., 2008. Nonlinear attenuation and rock damage during strong seismic ground motions, *Geochem. Geophys. Geosyst.*, 9, Q10015, doi:10.1029/2008GC002045.

Smith, E., & TenCate, J.A., 2000. Sensitive determination of the nonlinear properties of Berea sandstone at low strains, *Geophys. Res. Lett.*, 27, 1985–1988.

Stanchits, S., Vinciguerra, S., & Dresen, G., 2006. Ultrasonic velocities, acoustic emission characteristics and crack damage of basalt and granite, *Pure Appl. Geophys.*, 163, 975−994.

Sun, J. I., Golesorkhi, R., & Seed, H. B., 1988. Dynamic Moduli and Damping Ratios for Cohesive Soils, Report No. UCB/EERC-88/15, Earthquake Engineering Research Center, University of California, Berkeley, 42p.

TenCate, J.A., Pasqualini, D., Habib, S., Heitmann, K., Higdon, D., & Johnson, P. A., 2004. Nonlinear and nonequilibrium dynamics in geomaterials, *Phys. Rev. Lett.*, 93, doi:10.1103/Phys Rev Lett.93.065501.

Tsuda, K., Steidl, J., Archuleta, R., & Assimaki, D., 2006. Site-response estimation for the 2003 Miyagi-Oki earthquake sequence consider nonlinear site response. *Bull. Seismol. Soc. Am.*, 96, 1474–1482, doi:10.1785/0120050160.

Vucetic, M., & Dobry, R., 1991. Effect of soil plasticity on cyclic response, *J. Geotechnical Engineering Division*, ASCE, 111, 89–107.

Walsh, J.B., 1965. The effect of cracks on the uniaxial elastic compression of rocks, *J. Geophys. Res.* 70, 399– 411.

Weinberger, R., Reches, Z., Eidelman, A., & Scott, T.S., 1994. Tensile properties of rocks in four-point beam tests under confining pressure, in: *Proceedings First North American Rock Mechanics Symposium*, pp. 435–442, eds Nelson, P., & Laubach, S.E., Austin, Texas.

Winkler, K., Nur, A., & Gladwin, M., 1979. Friction and seismic attenuation in rocks, *Nature*, 277, 528–531.

Wu, C., Peng, Z., & Ben-Zion, Y., 2009. Non-linearity and temporal changes of fault zone site response associated with strong ground motion, *Geophys. J. Int.*, 176, 265–278, doi: 10.1111/j.1365-246X.2008.04005.x.

Zoback, M.D., & Byerlee, J.D., 1975. The effect of microcrack dilatancy on the permeability of Western granite, *J. Geophys. Res*. 80, 752–755.

Figure Captions

Figure 1. Results of strain-controlled uniaxial tension-compression tests on a composite prepared using lightly cross-linked poly-methyl methacrylate filled with alumina trihydrate (Basaran & Nie, 2004). Stress-strain cycles #5, 50, and 104 demonstrate gradual decrease in the elastic modulus under tension, while compressional part of the loop remains almost the same.

Figure 2. Acceleration versus frequency for different excitation levels (A) and normalized frequency shift versus acceleration (B) in Lavoux sandstone (from Johnson *et al.*, 1996).

Figure 3. Stress-strain cycles #104 from Figure 1; fit with linear damage model after Basaran & Nie (2004) and nonlinear damage model.

Figure 4. Schematic change of the stress-strain with damage. Bi-linear behavior incorporated in the nonlinear damage model allows significantly improve fitting to the experimental data (grey and red lines in Figure 3).

Figure 5. Simulated resonance curves under periodic forcing with amplitude from 100 to 5,000 Pa.

Figure 6. Simulated shift of the resonance frequency under different forcing; linear (a) and logarithmic (b) scale allows better demonstrate the system behavior under small and large forcing.

Figure 7. Simulated resonance amplitude for different forcing. Dash lines correspond to the amplitude-forcing relation expected for the linear system with constant quality factor.

Figure 8. Simulated resonance curves for the material damage from $\alpha=0$ to $\alpha=0.6$ and 100 Pa (a) and 10,000 Pa (b) periodic forcing. Note that the amplitude scale differs by factor of 50, while the forcing is increased by factor of 100. (c) A zoom in view of the small frequency range for the simulation with $\alpha=0.6$. Black lines represent the high forcing nonlinear case, while grey lines and grey scale on the right corresponds to the small forcing.

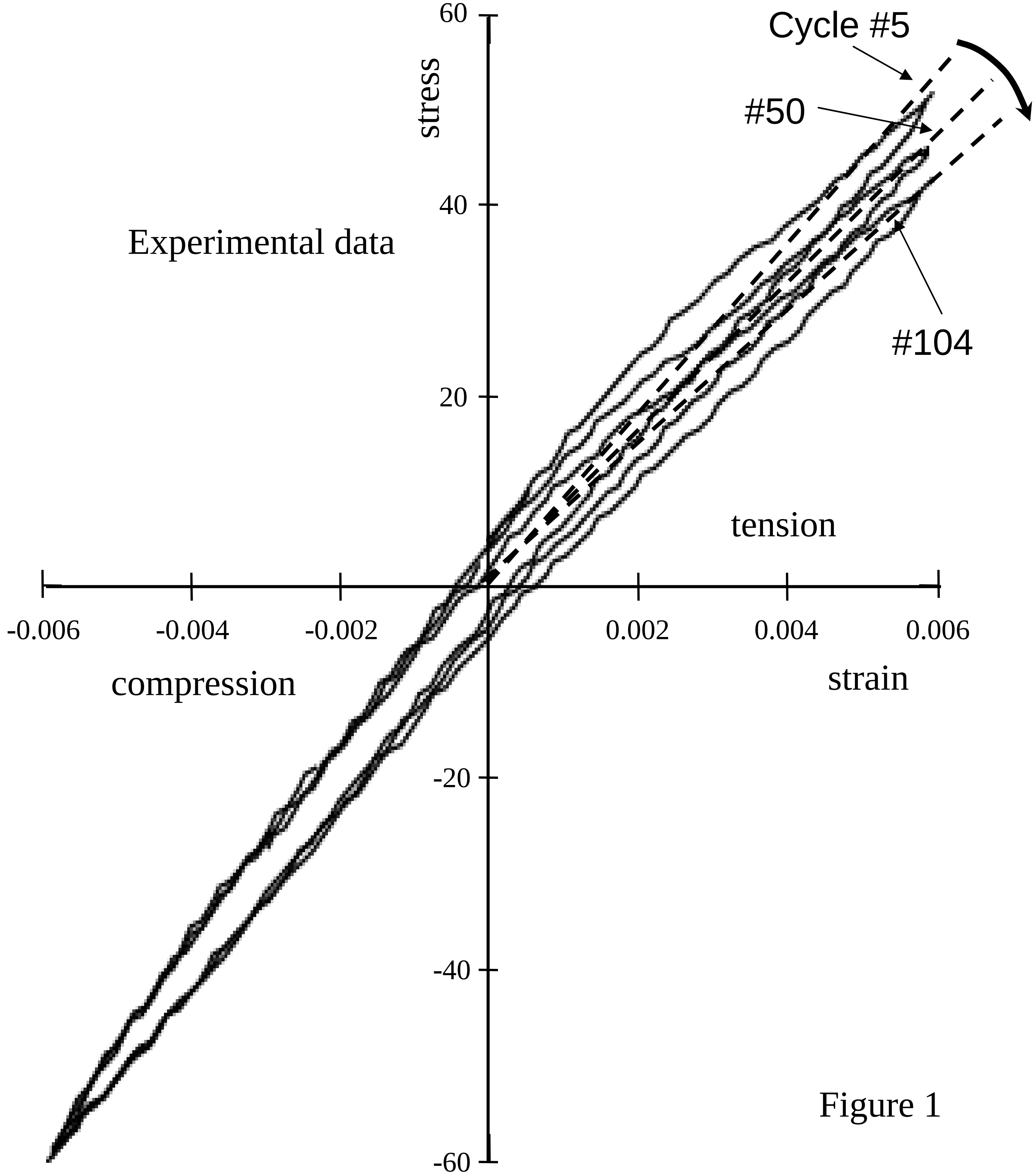

60
40
20
-20
-40
-60
stress
Cycle #5
#50
#104
Experimental data
tension
-0.006
-0.004
-0.002
0.002
0.004
0.006
strain
compression

Figure 1

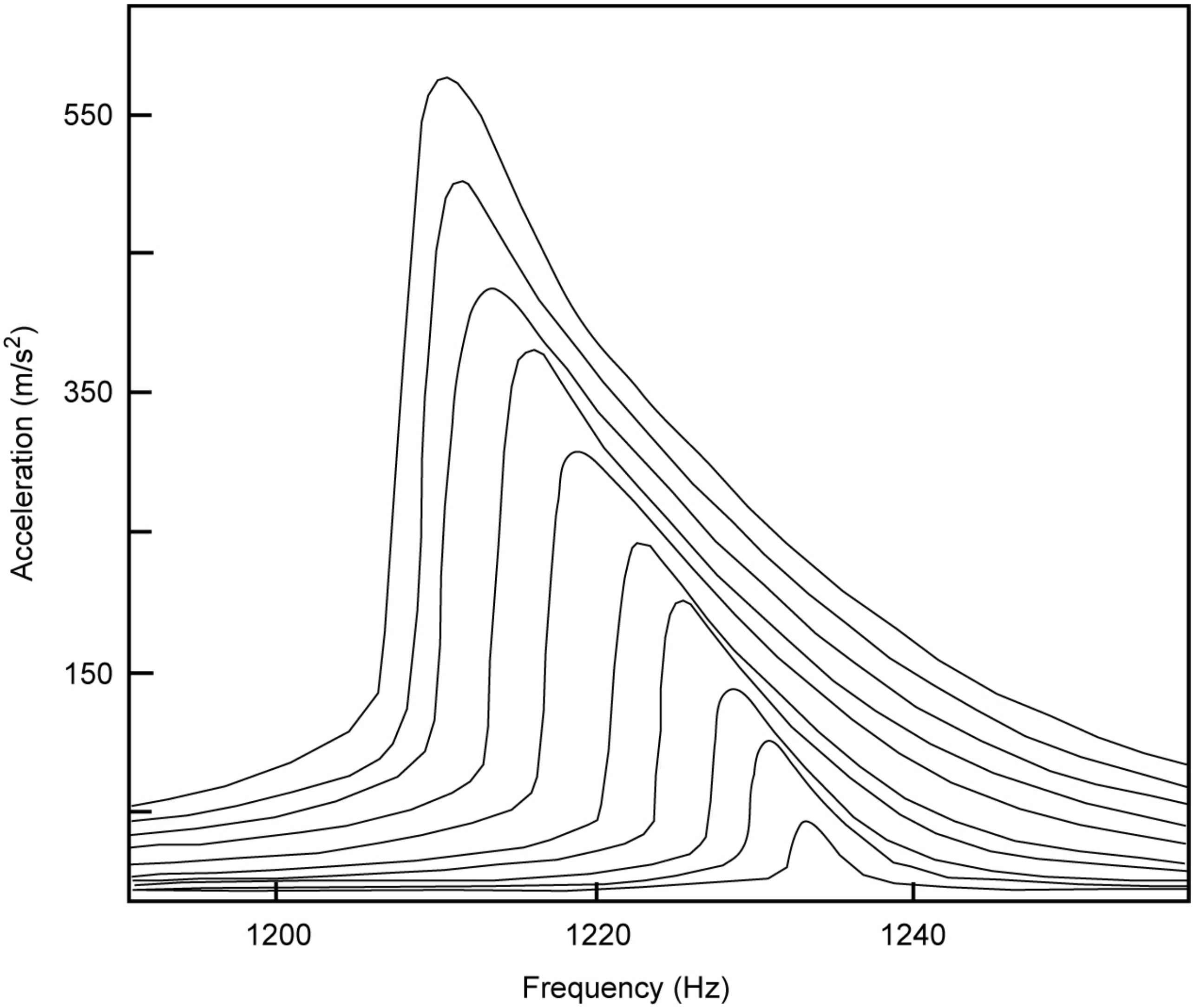

Figure 2a

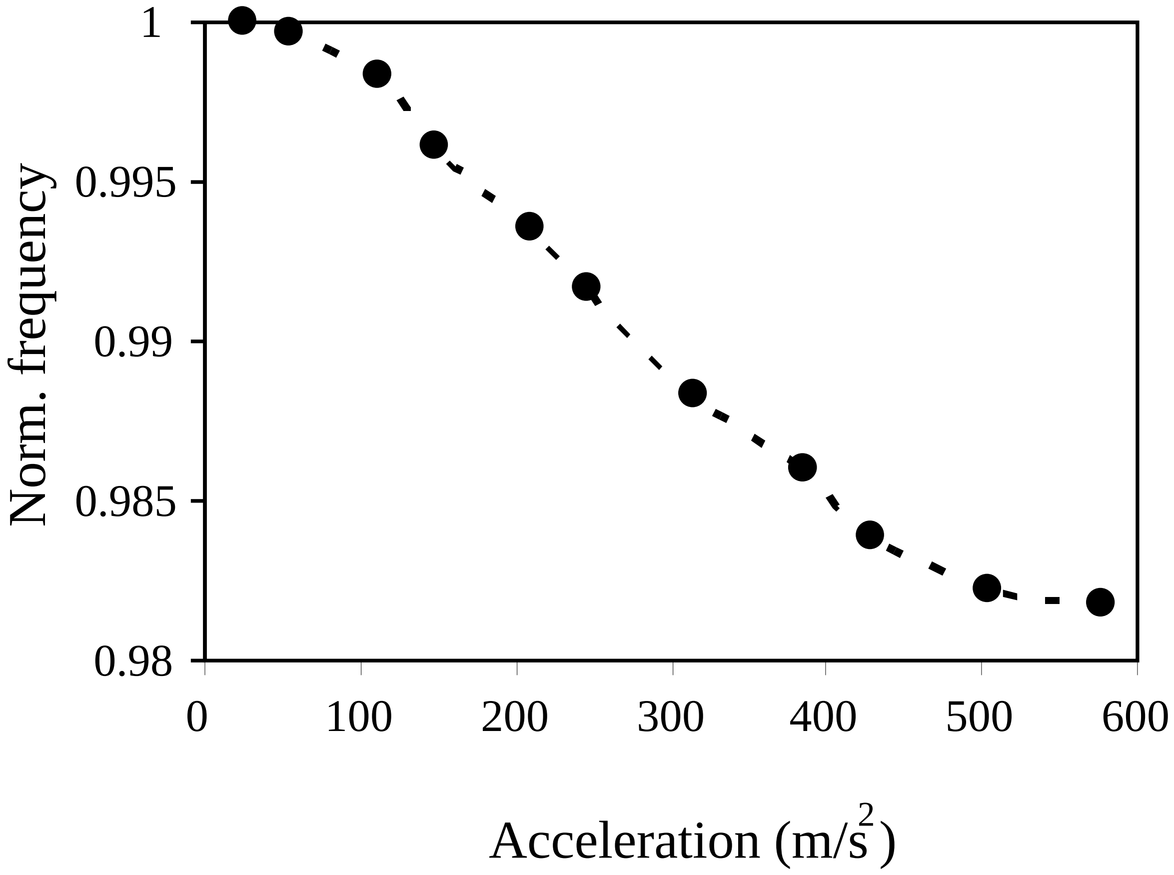

1
0.995
0.99
0.985
0.98
Norm. frequency
0
100
200
300
400
500
600
Acceleration (m/s^2)

Figure 2b

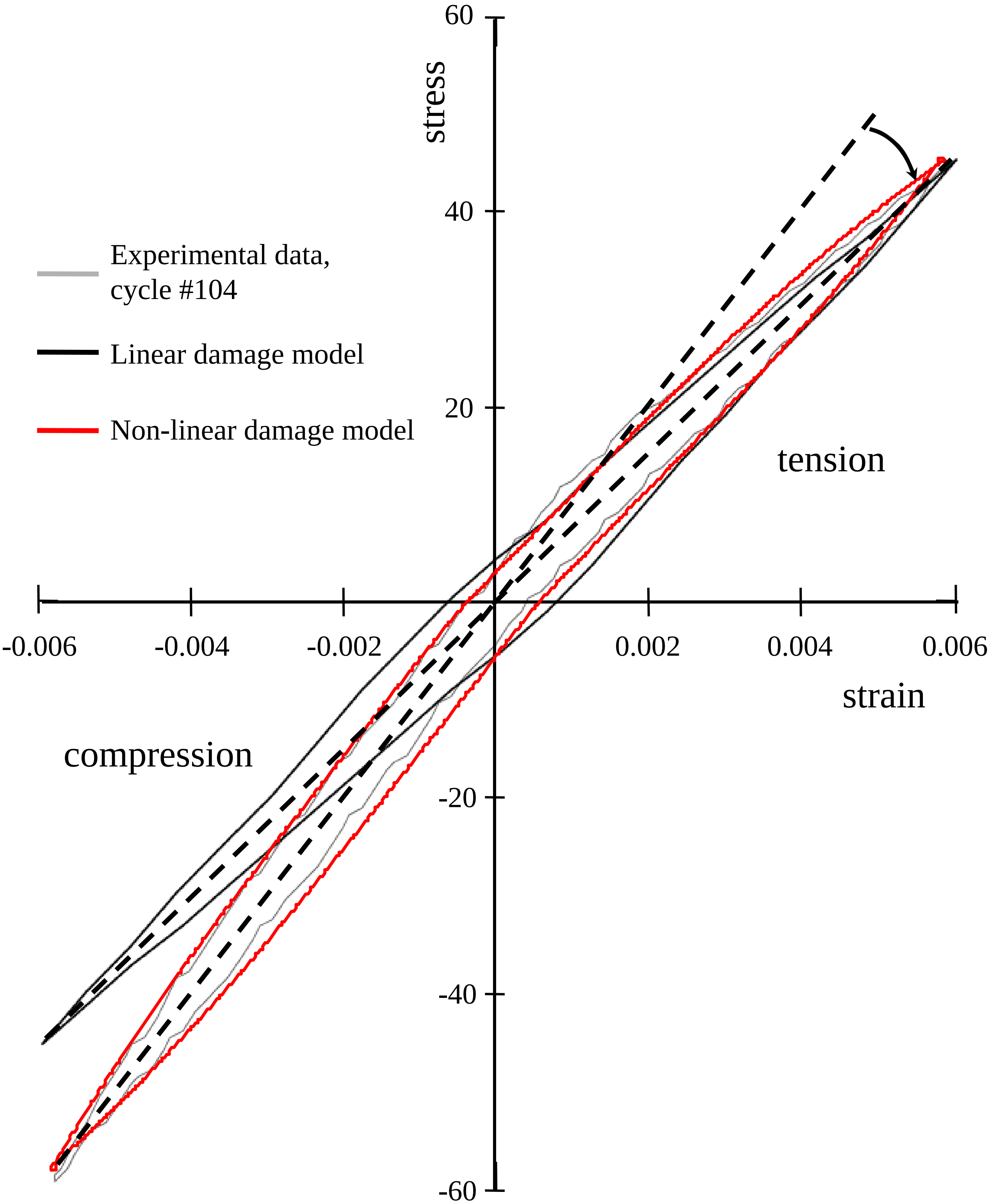

60
stress
40
Experimental data, cycle #104
Linear damage model
Non-linear damage model
20
tension
-0.006
-0.004
-0.002
0.002
0.004
0.006
strain
compression
-20
-40
-60

Figure 3

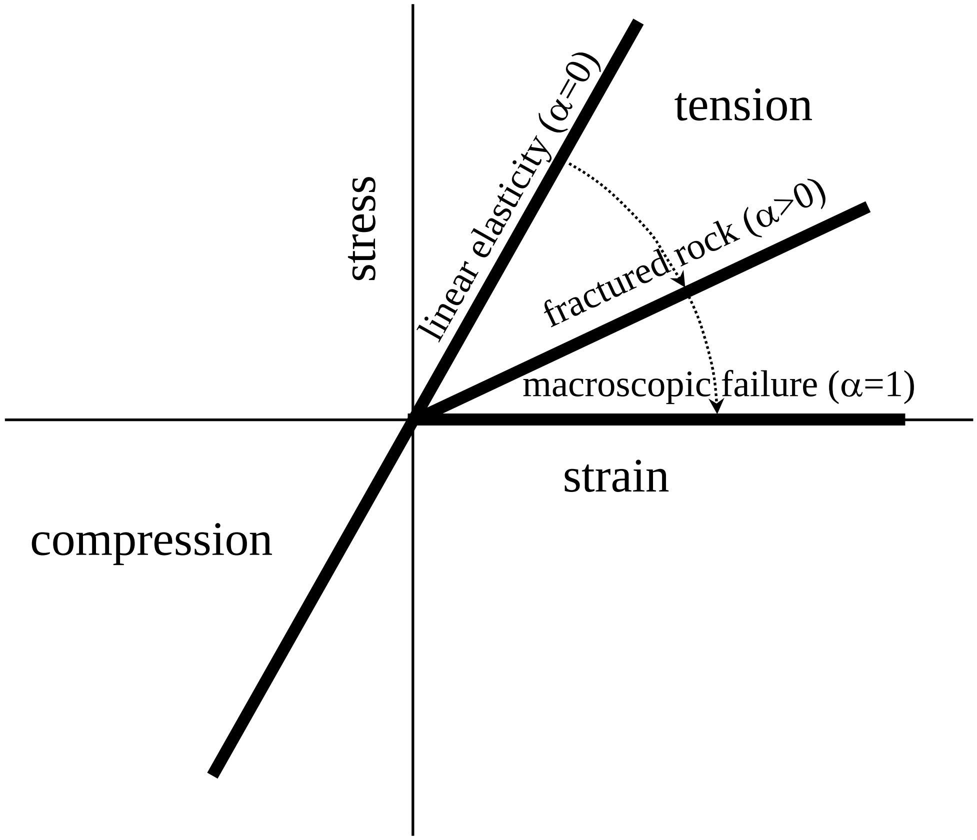
stress
linear elasticity (α=0)
tension
fractured rock (α>0)
macroscopic failure (α=1)
strain
compression

Figure 4

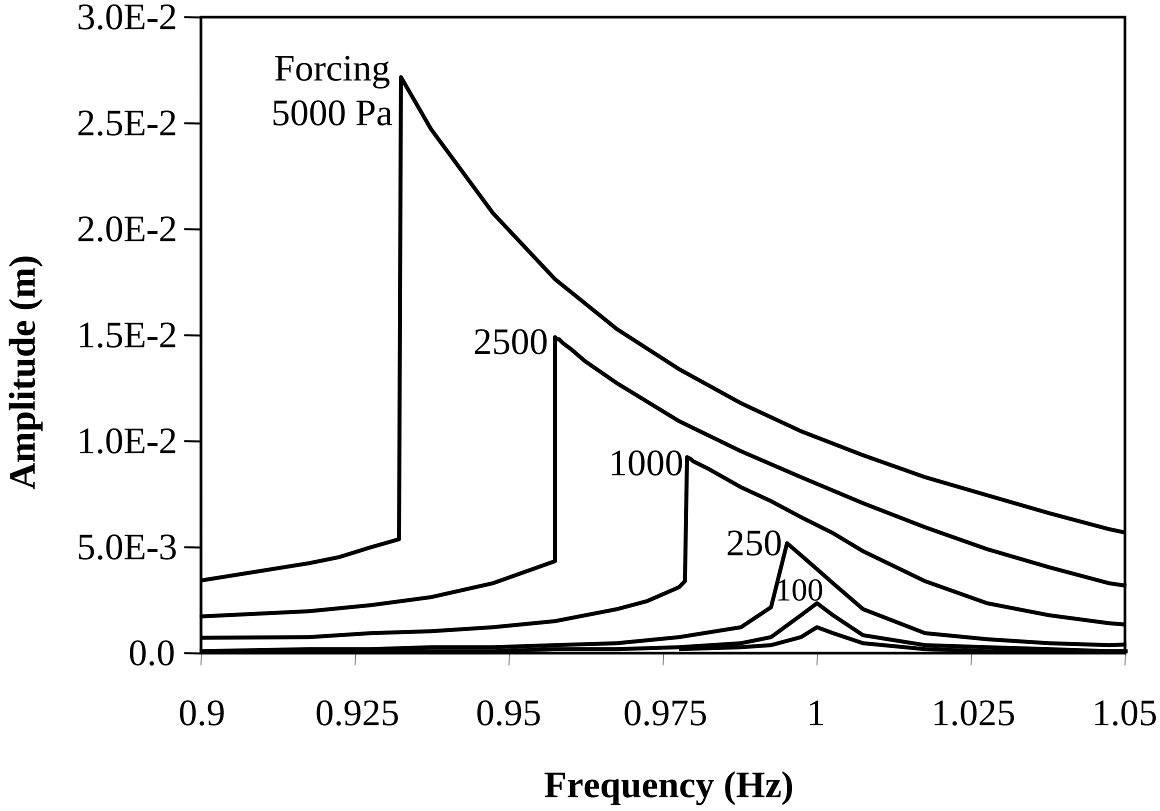
3.0E-2
2.5E-2
2.0E-2
1.5E-2
1.0E-2
5.0E-3
0.0
Amplitude (m)
Forcing
5000 Pa
2500
1000
250
100
0.9
0.925
0.95
0.975
1
1.025
1.05
Frequency (Hz)

Figure 5

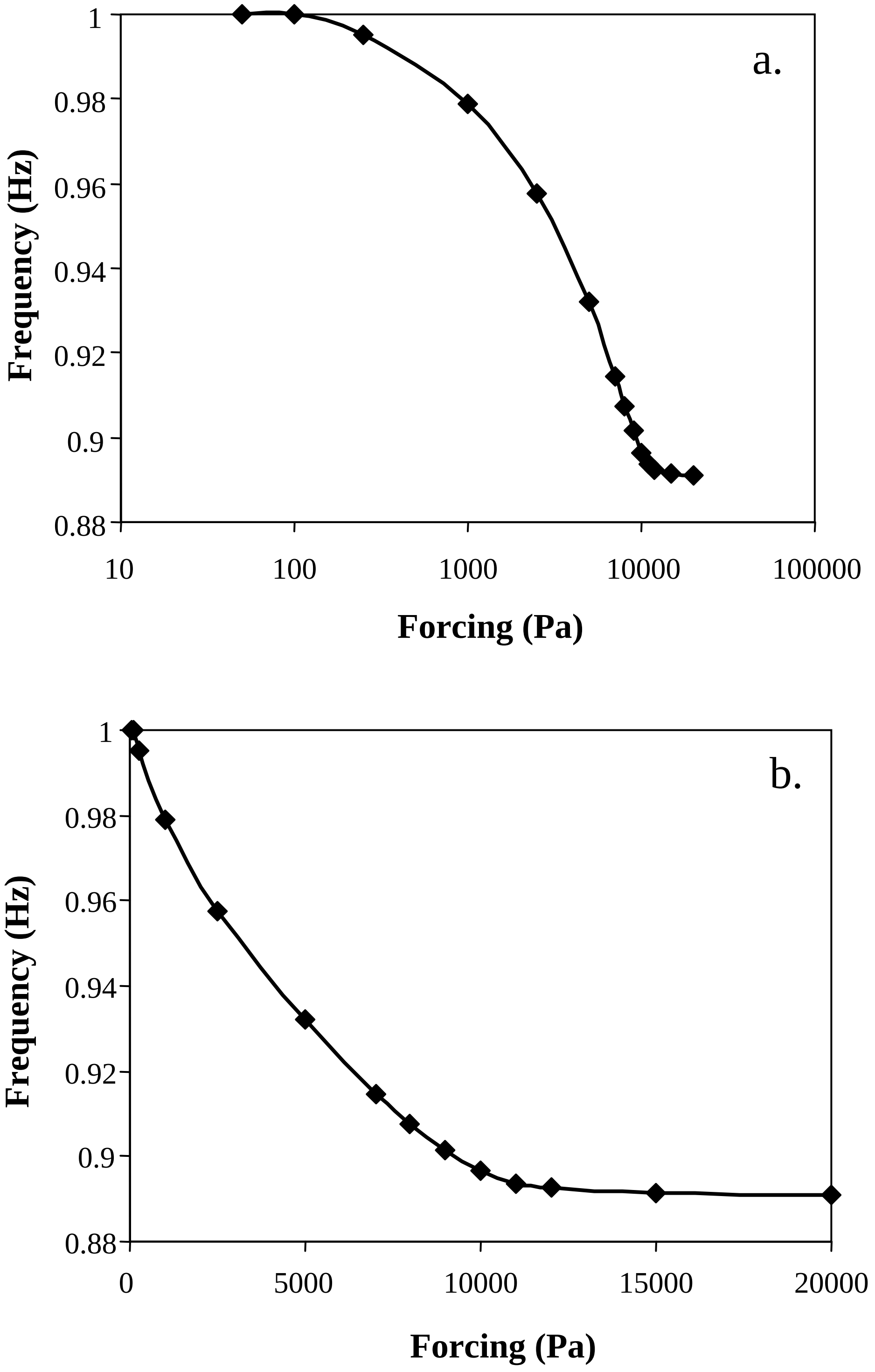

a.
Frequency (Hz)
1
0.98
0.96
0.94
0.92
0.9
0.88
10
100
1000
10000
100000
Forcing (Pa)
b.
Frequency (Hz)
1
0.98
0.96
0.94
0.92
0.9
0.88
0
5000
10000
15000
20000
Forcing (Pa)

Figure 6

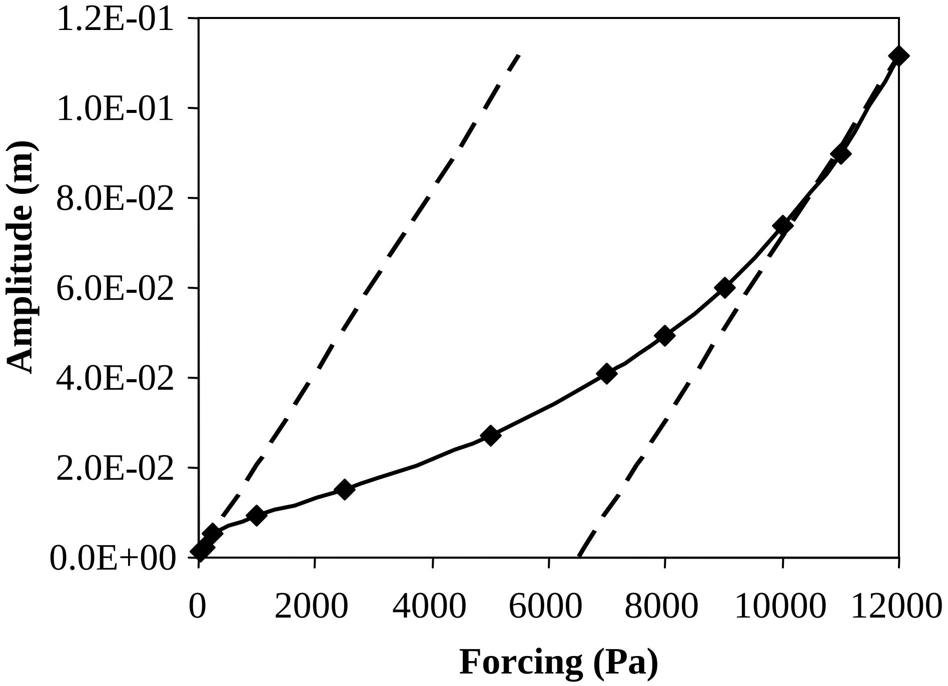
1.2E-01
1.0E-01
8.0E-02
6.0E-02
4.0E-02
2.0E-02
0.0E+00
Amplitude (m)
0
2000
4000
6000
8000
10000
12000
Forcing (Pa)

Figure 7

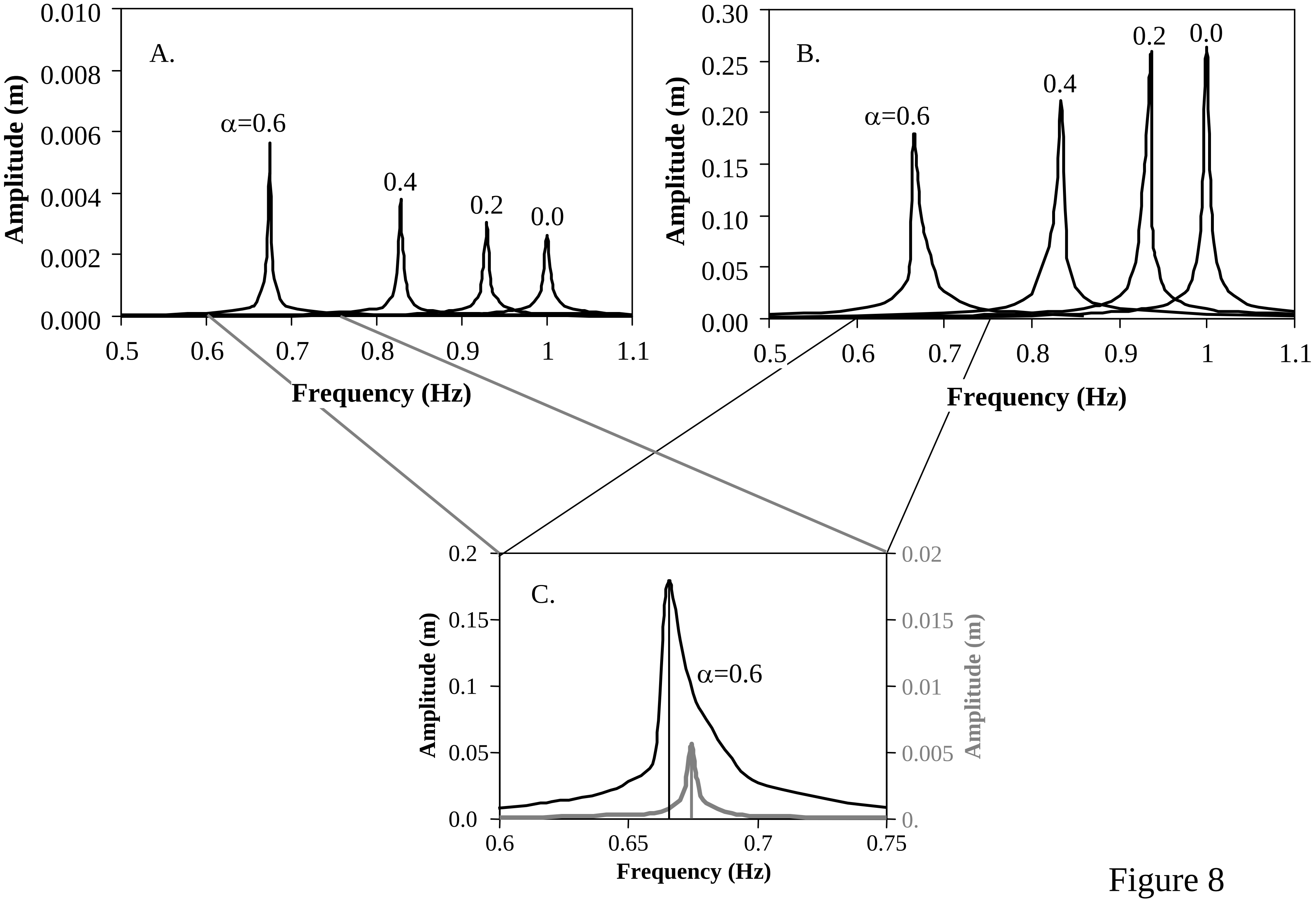
A.
Amplitude (m)
0.010
0.008
0.006
0.004
0.002
0.000
α=0.6
0.4
0.2
0.0
0.5
0.6
0.7
0.8
0.9
1
1.1
Frequency (Hz)
B.
Amplitude (m)
0.30
0.25
0.20
0.15
0.10
0.05
0.00
α=0.6
0.4
0.2
0.0
0.5
0.6
0.7
0.8
0.9
1
1.1
Frequency (Hz)
C.
Amplitude (m)
0.2
0.15
0.1
0.05
0.0
α=0.6
0.02
0.015
0.01
0.005
0.
Amplitude (m)
0.6
0.65
0.7
0.75
Frequency (Hz)

Figure 8